COMSOL
CONFERENCE
2023 MUNICH

Elastohydrodynamics of roll-to-plate nanoimprinting on non-flat substrates

J. Snieder[1,2], R.A.J. van Ostayen[1]
1. Department of Precision and Microsystems Engineering, Delft University of Technology, Delft, The Netherlands.
2. Morphotonics B.V., Veldhoven, The Netherlands.

Abstract
Roll-to-plate nanoimprinting is a replication technology to texture large-area substrates with UV-curable resins. A small and uniform film thickness is essential for many applications. Substrate non-flatness or waviness can cause undesired film thickness variations. The film thickness is a result of the hydrodynamic forces in the resin and the elastic forces of the flexible stamp and the elastomeric layer around the imprint roller. They combine into an elastohydrodynamic lubrication (EHL) system. This work presents an EHL model to study the film height on non-flat substrates. The numerical model is an extension of previous work. The substrate non-flatness is approximated with a cosine wave with a certain amplitude and wavelength. The results indicate that waviness of the substrate can have a significant impact on the film height. The variation of the film height will be most severe for large amplitude and a small wavelength substrate waviness.

Keywords: elastohydrodynamic lubrication, roll-to-plate nanoimprinting, film thickness, substrate waviness.

Introduction
Roll-to-plate nanoimprinting is a manufacturing method to replicate micro- and nanotextures on large-area substrates with UV-curable resins [1]. The nanoimprinted textures can enhance the functionality of the substrate in several ways by altering its optical or mechanical properties, such as anti-reflection or light-trapping films for solar panels and displays [2], [3], hydrophobic/oleophobic layers for self-cleaning or anti-fouling surfaces [4], and many more [5]. Figure 1 illustrates the Morphotonics roll-to-plate imprint process, which is considered in this study. It employs multiple rollers to both imprint and guide a textured, flexible stamp. A relatively soft, elastomeric layer surrounds the roller core to ensure conformal contact with the substrate. The imprint roller, positioned at the middle left, presses the flexible stamp into the UV-curable resin droplets. The droplets merge into a thin layer, which is solidified by UV-light. Upon delamination of the stamp, a negative of the textured pattern remains on the substrate. The final imprint consists of the desired texture on top of a residual layer, which ideally exhibits a small and uniform thickness across the entire substrate area. Typical film heights have a micrometer order of magnitude, but this can even be smaller.

Numerical simulation of the imprint process can assist in improving the predictability and uniformity of the film height. The film height is governed by the interaction of the hydrodynamic forces in the resin and the elastic forces of the flexible stamp and the elastomeric layer around the imprint roller. The physics and couplings are described by elastohydrodynamic lubrication (EHL) theory. In previous work, we developed an EHL model to study the film height as a function of the imprint process parameters [6]. The numerical model was experimentally validated and good agreement has been found between the results from simulation and experiment. However, the numerical model is only valid for flat substrates. In reality, the substrates are never perfectly flat. Substrate waviness will modify the roller contact zone, and hereby the pressure and film height profiles. Especially heat-treated or tempered glass substrates, which are used for solar panel production, can show significant substrate waviness. The local warp of rectangular substrates must not exceed 1.6 mm over any 300 mm span [7].

This work presents a numerical model to describe the physics of the roll-to-plate imprint process. The model is based on the previously developed EHL model and extended with substrate waviness. A detailed description of the implementation in COMSOL Multiphysics® is given [8]. The extended model can be used to study the impact of varying substrate waviness on the final film height.

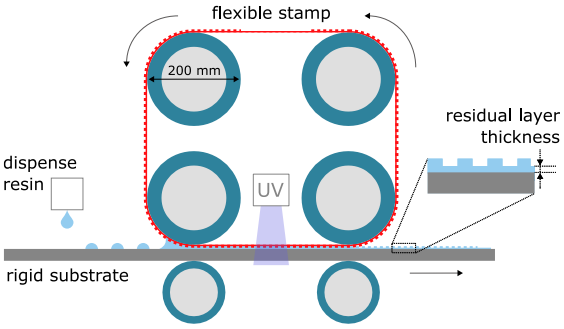

Figure 1. Schematic of the Morphotonics roll-to-plate imprint process. Reproduced and modified with permission from [6].

Methods

This section presents the model description with the governing equations and numerical implementation in COMSOL Multiphysics® to solve the EHL problem. The model is an extension of previous work [6], which is based on the model set-up presented by Habchi [9]. For sake of completeness, the modelling approach is summarized here as well, including modifications to take into account the substrate waviness.

Model description

A cross-section of the imprint roller can be seen on the top right of Figure 2. Typical parameter values are listed in Table 1. The roller with radius R is pressed onto the rigid, wavy substrate with an effective load F_L per unit length in z-direction. The waviness of the substrate is defined by a cosine function with amplitude a_s, wavelength λ_s, and phase shift φ_s. The flexible stamp, which is treated as a tensioned web with distributed web tension force T and distributed bending stiffness D, is assumed to be smooth and any textures are neglected in this study. It is partly wrapped around the roller and applies a contact pressure p_C onto the elastomeric layer with thickness d. Downstream the roller contact, the tensioned web loses contact with the roller and the gap g is formed. The roller/web and substrate are moving with an equal surface velocity of u_1 and u_2, respectively. They are separated by a thin film of resin with viscosity η and film height h. The film height of interest is the final layer height h_f. The hydrodynamic pressure build-up p is applied onto the tensioned web surface. Because the contact width is relatively small compared to the roller radius, a simplified equivalent geometry can be used, as shown on the bottom right in Figure 2. The elastomeric layer is unwrapped from the roller core and a rigid roller with a wavy surface around the nominal radius R is pressed into its surface. The equivalent geometry is described in a new coordinate system; the coordinates tangential and normal to the roller surface are represented by x' and z', respectively.

Table 1. Input parameters for numerical model.

Parameter	Value	Unit
F_L	2000	N/m
η	100	mPa s
R	100	mm
E	3	MPa
ν	0.45	-
u_1 & u_2	10.6	mm/s
d	9.9	mm
D	0.01	N m
T	464.3	N/m

The model is governed by five main equations, which are solved simultaneously; the linear elasticity equations, Reynolds equation, large-deflection bending of thin plates equation, the Fischer–Burmeister constraint function used to determine the contact between roller and stamp, and a load balance equation. They are shown on the left in Figure 2, including the couplings between them. A quasi-static solution procedure is employed, which is valid even for a varying substrate curvature, given the slow nature of the nanoimprint process. The model is written in dimensionless form. The following dimensionless variables are used in the description of the equations:

$$P = \frac{p}{p_\mathrm{h}}, \quad P_\mathrm{C} = \frac{p}{p_\mathrm{h}}, \quad W_\mathrm{W} = \frac{w_\mathrm{W} R}{a_\mathrm{h}^2},$$
$$U = \frac{uR}{a_\mathrm{h}^2}, \quad W = \frac{wR}{a_\mathrm{h}^2}, \quad A_\mathrm{s} = \frac{a_\mathrm{s} R}{a_\mathrm{h}^2},$$
$$G = \frac{gR}{a_\mathrm{h}^2}, \quad H = \frac{hR}{a_\mathrm{h}^2}, \quad \Lambda_\mathrm{s} = \frac{\lambda_\mathrm{s}}{a_\mathrm{h}},$$
$$X' = \frac{x'}{a_\mathrm{h}}, \quad Z' = \frac{z'}{d}, \quad \Phi_\mathrm{s} = \frac{\varphi}{a_\mathrm{h}},$$
$$K = R\kappa,$$

with the dimensionless hydrodynamic pressure P, contact pressure P_C, elastic deformation of the tensioned web W_W, elastic deformation components U and W of the elastomeric layer, substrate waviness amplitude A_s, gap G, film height H, substrate waviness wavelength Λ_s, spatial coordinates X' and Z', substrate waviness phase shift Φ_s, and tensioned web curvature K. The Hertz dry contact half-width a_h and peak pressure p_h for a line contact are used for scaling. These are based on the mechanical properties of the elastomeric layer:

$$a_\mathrm{h} = \sqrt{\frac{8F_\mathrm{L}R}{\pi E'}},$$
$$p_\mathrm{h} = \frac{2F_L}{\pi a_\mathrm{h}}.$$

It is assumed all deformation occurs in the relatively soft elastomeric layer, so the effective elastic modulus E' is given by:

$$\frac{2}{E'} = \frac{1-\nu^2}{E},$$

with Poisson ratio ν and elastic modulus E. The equations are applied on the computational domain in Figure 3. It has a dimensionless length of 20 and dimensionless height of 1. The roller center is located at $X' = 0$.

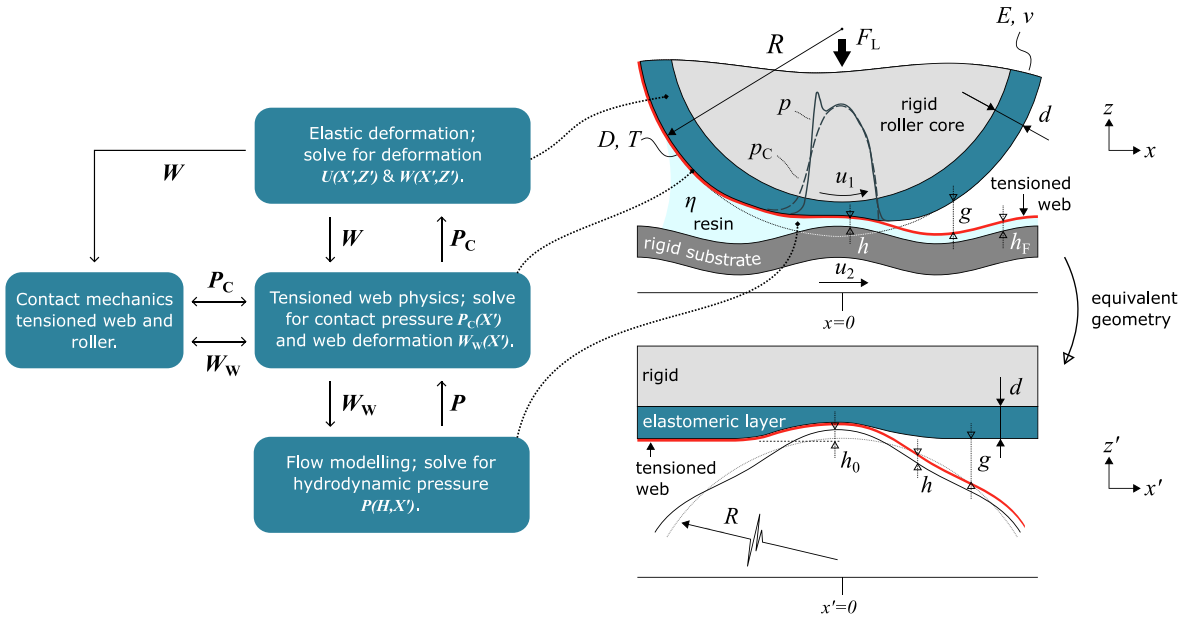

Figure 2. Left: physics of the EHL model and couplings between them. Top right: schematic of the imprint roller including parameters. Bottom right: equivalent geometry of the imprint roller. Reproduced and modified with permission from [6].

The elastic deformation of the elastomeric layer is determined via the dimensionless linear elasticity equations, which are given by:

$$\begin{aligned}&\frac{\partial}{\partial X'}\left[(\lambda+2\mu)\frac{d}{a_\mathrm{h}}\frac{\partial U}{\partial X'}+\lambda\frac{\partial W}{\partial Z'}\right]\\&+\frac{\partial}{\partial Z'}\left[\mu\left(\frac{a_\mathrm{h}}{d}\frac{\partial U}{\partial Z'}+\frac{\partial W}{\partial X'}\right)\right]=0,\\&\frac{\partial}{\partial X'}\left[\mu\left(\frac{\partial U}{\partial Z'}+\frac{d}{a_h}\frac{\partial W}{\partial X'}\right)\right]\\&+\frac{\partial}{\partial Z'}\left[\lambda\frac{\partial U}{\partial X'}+(\lambda+2\mu)\frac{a_h}{d}\frac{\partial W}{\partial Z'}\right]=0.\end{aligned}\qquad(1)$$

The parameters λ and μ represent the Lamé parameters, which are defined by:

$$\lambda=\frac{\nu E_\mathrm{eq}}{(1-2\nu)(1+\nu)},$$

$$\mu=\frac{E_\mathrm{eq}}{2(1+\nu)},$$

with the equivalent elastic modulus of the elastomeric layer [10]:

$$E_\mathrm{eq}=E\frac{a_\mathrm{h}}{Rp_\mathrm{h}}.$$

The equations are applied on domain Ω in Figure 3 and the contact pressure P_C is applied on domain boundary $\partial\Omega_\mathrm{C}$, using these boundary conditions:

$$\begin{aligned}&U=W=0 && \text{on } \partial\Omega_\mathrm{T},\\&U=0 && \text{on } \partial\Omega_\mathrm{L} \text{ and } \partial\Omega_\mathrm{R},\\&\sigma_\mathrm{n}=P_\mathrm{c} && \text{on } \partial\Omega_\mathrm{C},\\&\sigma_\mathrm{n}=\sigma_\mathrm{t}=0 && \text{elsewhere.}\end{aligned}$$

The parameters σ_n and σ_t are the normal and tangential stress tensor components, respectively.

The resin flow between the tensioned web and the substrate is described by lubrication theory. The pressure build-up in the thin film of resin is determined with the dimensionless, incompressible, steady-state Reynolds equation in 1D [11]:

$$\frac{\partial}{\partial X'}\left(-\frac{a_\mathrm{h}^3 p_\mathrm{h}}{12R^2\eta(u_1+u_2)}H^3\frac{\partial P}{\partial X'}+\frac{H}{2}\right)=0.\qquad(2)$$

The Reynolds equation is applied on domain boundary $\partial\Omega_\mathrm{H}$. The following boundary conditions are applied:

$$\begin{aligned}&P=0 && \text{at } X'=-4.5,\\&\frac{\partial P}{\partial X'}=\frac{H}{2} && \text{at } X'=10.\end{aligned}$$

In contrast to previous work [6], the Neumann boundary condition at the right domain boundary describes a continuation of the resin flow via the convection term in the Reynolds equation. The dimensionless film height is described by the difference between the surfaces of the tensioned web and substrate, which now shows a non-flatness:

$$H=H_0+H_\mathrm{W}+W_\mathrm{W}-H_\mathrm{sub},$$

$$H_\mathrm{W}=\begin{cases}\dfrac{X'^2}{2}, & X'\le 0,\\ 0, & X'>0,\end{cases}$$

$$H_\mathrm{sub}=A_\mathrm{s}\cos\left(\frac{2\pi}{\Lambda_\mathrm{s}}(X'-\Phi_\mathrm{s})\right).$$

The constant H_0 represents the offset or roller engagement, as indicated in Figure 2. It will be determined with the load balance equation.

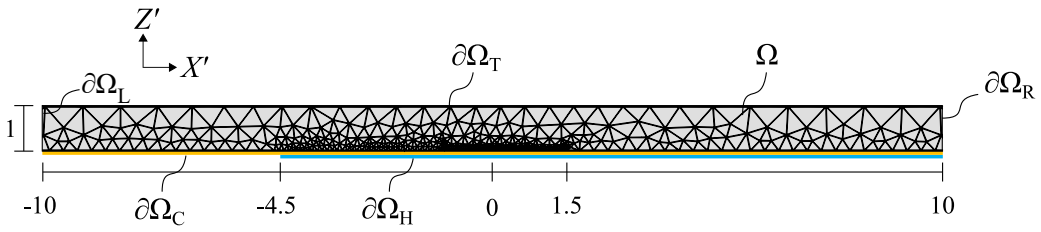

Figure 3. Dimensionless computational domain and mesh. Reproduced and modified with permission from [6].

The tensioned web is characterized by its initial shape H_W and its elastic deformation W_W, which follows from Equation (3). The web partly follows the roller surface, which is approximated with a parabolic function. The waviness of the substrate surface is described by a cosine function. By varying the phase shift Φ_s, the motion of the substrate can be simulated in a quasi-static manner. Moreover, it is assumed that the resin can handle small negative pressures and cavitation is not included [6]. The film height between the roller surface and substrate is also defined:

$$H_\mathrm{roller} = H_0 + \frac{X'^2}{2} + W - H_\mathrm{sub}.$$

The elastic deformation of the tensioned web is determined with the Föppl–von Kármán equations, which describe the large-deflection bending of thin plates under tension and pressure [12]:

$$\left(-\frac{D}{a_\mathrm{h}^2 p_\mathrm{h} R}\right)\frac{\partial^2 K}{\partial X'^2} + \left(\frac{T}{p_\mathrm{h} R}\right)K + P_\mathrm{n} = 0. \qquad (3)$$

The normal pressure P_n is defined by the difference between the hydrodynamic pressure and the contact pressure, which are both acting on the web: $P_\mathrm{n} = P - P_\mathrm{C}$. The web curvature K is approximated by the second spatial derivative of the web shape:

$$K = \frac{\partial^2}{\partial X'^2}(H_\mathrm{W} + W_\mathrm{W}) \qquad (4)$$

$$= \begin{cases} 1 + \dfrac{\partial^2 W_\mathrm{W}}{\partial X'^2}, & X' \le 0, \\ \dfrac{\partial^2 W_\mathrm{W}}{\partial X'^2}, & X' > 0. \end{cases}$$

The bending stiffness of the tensioned web is defined by its thickness t, elastic modulus E_W, and Poisson's ratio ν_W:

$$D = \frac{E_\mathrm{W} t^3}{12(1-\nu_\mathrm{W}^2)}.$$

Equation (3) and Equation (4) are applied on domain boundary $\partial\Omega_\mathrm{C}$. Due to the presence of substrate waviness, the boundary conditions at the right side of the domain at $X' = 10$ will be defined explicitly. It is assumed that the tensioned web will adopt the substrate direction and curvature on this location. This is implemented via two Neumann boundary conditions:

$$\left.\frac{\partial W_\mathrm{W}}{\partial X'}\right|_{X'=10} = \left.\frac{\partial H_\mathrm{sub}}{\partial X'}\right|_{X'=10}$$

$$= -A_\mathrm{s}\left(\frac{2\pi}{\Lambda_\mathrm{s}}\right)\sin\left(\frac{2\pi}{\Lambda_\mathrm{s}}(X' - \Phi_\mathrm{s})\right)\Bigg|_{X'=10}$$

$$\left.\frac{\partial K}{\partial X'}\right|_{X'=10} = \left.\frac{\partial^3 H_\mathrm{sub}}{\partial X'^3}\right|_{X'=10}$$

$$= A_\mathrm{s}\left(\frac{2\pi}{\Lambda_\mathrm{s}}\right)^3 \sin\left(\frac{2\pi}{\Lambda_\mathrm{s}}(X' - \Phi_\mathrm{s})\right)\Bigg|_{X'=10}$$

The contact mechanics between the tensioned web and the roller surface are described by the contact pressure P_C and the gap G, which can be combined in a complementarity condition. A contact pressure will be present when the gap is zero. And vice versa, if the contact pressure is zero, the gap will be larger than zero:

$$P_\mathrm{C} \ge 0 \text{ and } G = 0,$$
$$P_\mathrm{C} = 0 \text{ and } G \ge 0.$$

The gap is defined by:

$$G = G_0 + W - W_\mathrm{W}$$

$$G_0 = \begin{cases} 0, & X' \le 0, \\ \dfrac{X'^2}{2}, & X' > 0. \end{cases}$$

The term G_0 is the initial gap between the web and roller. It increases with the approximated roller shape for $X' > 0$. The complementarity condition is solved by a Fischer–Burmeister constraint function, which is applied on domain boundary $\partial\Omega_\mathrm{C}$ [13]:

$$P_c + G - \sqrt{{P_c}^2 + G^2} = 0 \qquad (5)$$

The hydrodynamic pressure build-up must be in equilibrium with the applied effective load. The dimensionless load balance equation is given by:

$$\int_{\partial\Omega_\mathrm{H}} P \,\mathrm{d}X' = \frac{\pi}{2}. \qquad (6)$$

This equation is satisfied by adjusting the offset H_0 in the definition of the film height.

Implementation in COMSOL Multiphysics®

The equations combine into an EHL model, which is implemented in COMSOL Multiphysics®. They are applied on different parts of the computational domain in Figure 3, as specified in the previous section. The computational domain also shows the mesh, of which the size varies over the lower domain boundary, see Table 2. A *free triangular mesh* is employed in domain Ω. The mesh is refined near the center, where the largest pressure and film height gradients will be present. In contrast to previous work, the boundary with the finest mesh is extended because the location of the pressure and film height profiles will slightly vary, due to the substrate waviness.

Table 2. Mesh settings.

Domain / boundary	Location	Mesh size
Ω	entire domain	coarser
$\partial\Omega_C$	$-10 < X' < -4.5$ $1.5 < X' < 10$	max. 0.3
$\partial\Omega_C$	$-4.5 < X' < -1$	max. 0.1
$\partial\Omega_C$	$-1 < X' < 0.5$	max. 0.02
$\partial\Omega_C$	$0.5 < X' < 1.5$	max. 0.01

The linear elasticity equations in Equation (1) are implemented via the *Weak Form PDE interface* with the elastic deformation components U and W as dependent variables [14]. The boundary conditions are added via two *Dirichlet Boundary Conditions* and the contact pressure is implemented via a *Boundary Flux/Source* term. The equations are discretized with third-order (cubic) elements. The initial solution for the elastic deformation is determined by applying the dimensionless Hertz pressure distribution on the contact domain boundary:

$$P_{\text{initial}} = P_{\text{Hertz}} = \begin{cases} \sqrt{(1 - X'^2)}, & -1 \le X' \le 1, \\ 0, & \text{elsewhere.} \end{cases}$$

The Reynolds equation in Equation (2) is implemented via the *General Form Boundary PDE interface*. The dependent variable is the hydrodynamic pressure P. The left boundary condition at $X' = -4.5$ is implemented via a *Dirichlet Boundary Condition* while the right boundary condition at $X' = 10$ is implemented via a *Flux/Source* node. Second-order (quadratic) elements are used for discretization. The hydrodynamic pressure is initialized with the dimensionless Hertz pressure distribution. The load balance is added via a *Global Equation*, which solves for the film height offset H_0. The initial value is set to a small positive number, to ensure a feasible starting point for the solver.

The large-deflection bending of thin plates equations in Equation (3) and (4) and the Fischer–Burmeister constraint function in Equation (5) are implemented together via another *General Form Boundary PDE interface*, with dependent variables W_W, K, and P_C. Because of the nested fourth order spatial derivative in Equation (3), the implementation is achieved via two second order PDEs. The boundary conditions for the large-deflection bending of thin plates equations are implemented via a *Flux/Source* term. The equations are discretized with third-order (cubic) elements, and the curvature K is initialized with the dimensionless roller curvature:

$$K_{\text{initial}} = \begin{cases} 1, & X' \le 0, \\ 0, & X' > 0. \end{cases}$$

The initial contact pressure is partly based on the dimensionless Hertz pressure distribution and the contribution of the tensioned web itself:

$$P_{\text{C,initial}} = \begin{cases} \dfrac{T}{p_h R} + \sqrt{(1 - X'^2)}, & X' \le 0, \\ 0, & X' > 0. \end{cases}$$

The set of equations are solved in a fully-coupled manner in Comsol Multiphysics® using two stationary study steps. The first study step is only involved with the calculation of the elastic deformation of the elastomeric layer, which follows from applying the dimensionless Hertz pressure distribution on the contact domain boundary. The result is used as initial solution in the secondary study step. The model is then iteratively solved until convergence. The final film height H_f is evaluated at the end of the domain boundary $\partial\Omega_H$ at $X' = 10$.

Results and discussion

The numerical model is solved for the input parameters in Table 1 and a variation of the substrate waviness parameters. These are benchmarked at a dimensionless amplitude A_s of 1 and a dimensionless wavelength Λ_s of 15, which correspond to a dimensional value of 0.68 mm and 123 mm, respectively. The phase shift Φ_s is varied as a fraction of the wavelength, hereby effectively moving the wavy substrate underneath the roller and web. Figure 4 shows the simulated height profiles of the roller, tensioned web and substrate on (non-)flat substrates for a variation of the phase shift. The phase shift of $\Phi_s = 0$ and $\Phi_s = \Lambda_s/2$ correspond to a peak or valley at the roller center, respectively. The actual film heights H, which are defined as the distance between the tensioned web and substrate surface, are too small to distinguish. The figure clearly shows that the tensioned web follows the roller surface up to the outlet, after which it moves along with the substrate surface and the roller surface diverges. Both roller and web deform conform to the substrate surface, which results in a modified contact zone. The presence of a peak at the roller center

results in a reduced contact zone, while the presence of a valley at the roller center results in an increased contact zone, compared to the flat substrate case.

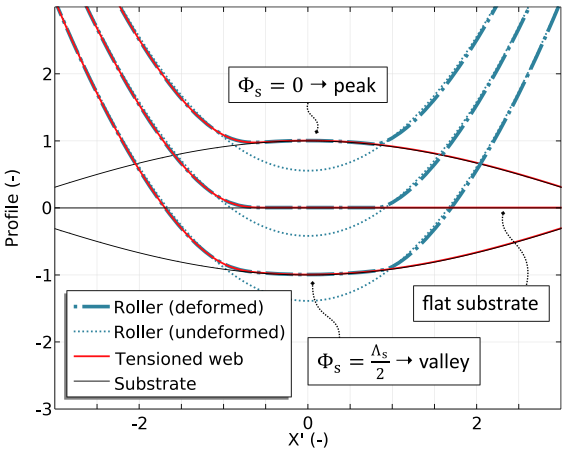

Figure 4. Height profiles of the roller, tensioned web and substrate for on (non-)flat substrates for a variation of the phase shift ($\Phi_s = 0$ → peak and $\Phi_s = \Lambda_s/2$ → valley).

The actual film heights and corresponding pressure profiles are shown in Figure 5 to Figure 7. For a detailed explanation about the EHL behavior of the roll-to-plate imprint process with tensioned webs, the reader is referred to our previous publication [6]. The profiles on a flat substrate can be seen in Figure 5. The Hertz pressure and roller height profile are shown for reference. In front of the contact zone, the tensioned web exerts a contact pressure on the roller surface. The hydrodynamic pressure is negligible in this region. Towards the roller center, both contact pressure and hydrodynamic pressure increase. The hydrodynamic pressure peak just before the roller center can be explained by the bending stiffness of the tensioned web, which causes the web to deform towards the substrate surface, hereby forming a constriction for the resin flow. After the roller center, the pressures decrease to ambient pressure. The corresponding film height profile decreases due to the converging roller surface, and stays more or less constant in the contact zone. The tensioned web follows the roller surface until the outlet, after which they lose contact. A uniform film height can be found, which represents the final film height H_f.

Figure 6 shows the pressure and film height profiles on a non-flat substrate surface for a phase shift Φ_s equal to zero. The decreased contact area results in an increase of the pressure profiles and a decrease of the corresponding film height profiles, compared to the flat substrate scenario. Therefore, the final film height is smaller. The opposite is true for a phase shift Φ_s equal to $\Lambda_s/2$, which is shown in Figure 7. The contact area is increased, and as a result, the pressure profiles are decreased and the film height profiles are increased. The final film height is now larger compared to the value on a flat substrate.

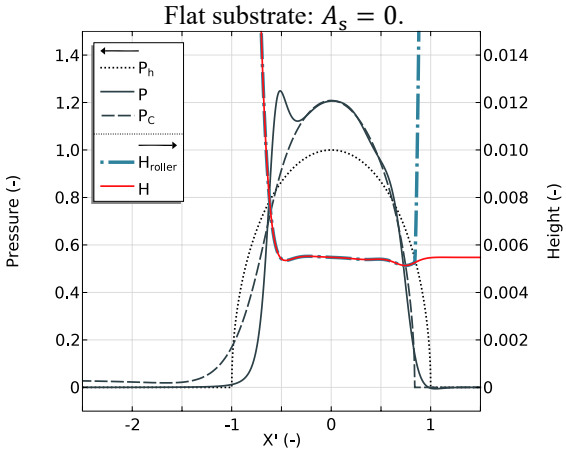

Figure 5. Pressure and film height profiles on a flat substrate surface.

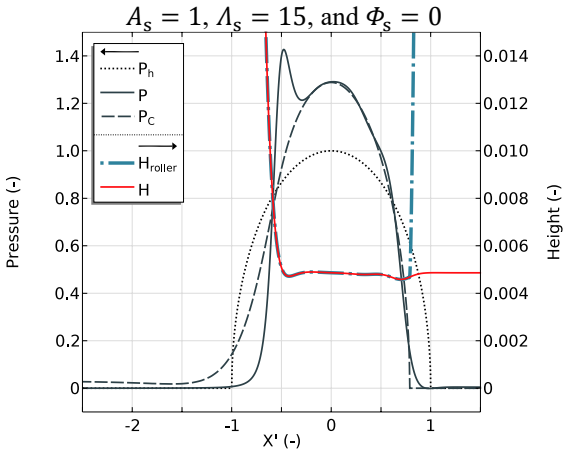

Figure 6. Pressure and film height profile on a non-flat substrate surface. A peak is located at the roller center.

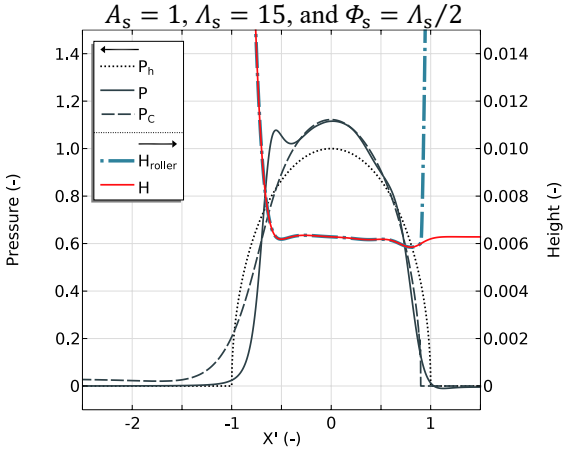

Figure 7. Pressure and film height profile on a non-flat substrate surface. A valley is located at the roller center.

The last study in Figure 8 presents the final film height for a variation of the substrate waviness amplitude, wavelength and phase shift. Dimensional values are presented, to give the reader a sense of the order of magnitude. The nominal film height on a flat substrate is equal to 3.71 µm. The top graph shows that the film height changes for a variation of the phase shift, which increases from zero to a full wavelength. A repetitive pattern can be recognized, which corresponds the results in Figure 6 and

Figure 7. The final film height is smaller than nominal when the peak is located near the roller center, and larger than nominal when the valley is located near the roller center. The deviation increases for increasing substrate waviness amplitude. The figure at the bottom of Figure 8 shows the final film height for a variation of the wavelength. Again, the final film height is either smaller or larger compared to the nominal value, depending on the presence of a peak or valley at the location of the roller center. The deviation from the nominal value is largest for small wavelengths and large amplitude. The difference diminishes for increasing wavelength, when the contact width becomes negligibly small compared to the wavelength of the substrate waviness.

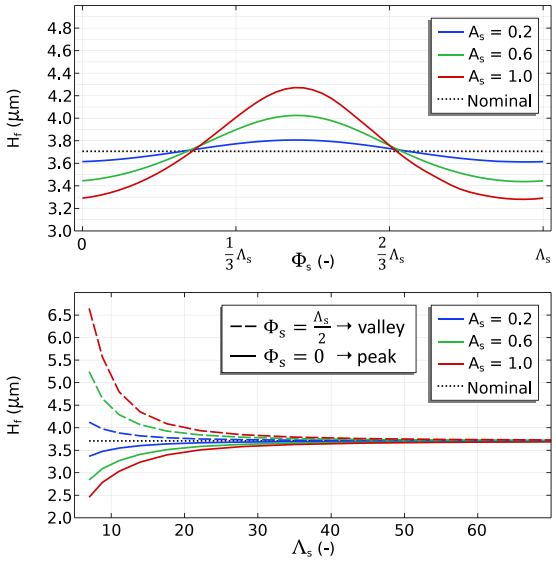

Figure 8. Top: final film height for a variation of substrate waviness amplitude and phase shift. Bottom: final film height for a variation of substrate waviness amplitude, phase shift ($\Phi_s = 0$ and $\Phi_s = \Lambda_s/2$), and wavelength.

Conclusion

A numerical EHL model, which is an extension of previous work, is developed to study the film height on non-flat substrates. The model combines several physics to describe the elastic deformation and contact mechanics of the elastomeric layer and tensioned web around the roller and the fluid flow of the thin film of resin between the tensioned web and the substrate. The results show that the substrate waviness can have a significant impact on the final film height. The deviation from the nominal case, which is defined as the film height on a flat substrate, is most severe for large amplitude and small wavelength substrate waviness. The numerical model can be used to study the influence of the process parameters on the final film height in the presence of substrate waviness. These insights can be used to design new imprint systems, to make them more robust to substrate waviness and to further improve the imprint quality.

References

[1] H. Schift and A. Kristensen, "Nanoimprint Lithography," in *Springer Handbook of Nanotechnology*, B. Bhushan, Ed., in Springer Handbooks. , Berlin, Heidelberg: Springer, 2007, pp. 239–278. doi: 10.1007/978-3-540-29857-1_8.

[2] C. Ji *et al.*, "Lenticular-Lens-Based Colored Antiglare Dashboard Surfaces," *Advanced Materials Technologies*, vol. 2, pp. 1–7, Nov. 2016, doi: 10.1002/admt.201600177.

[3] L. Clasing, D. Werner-Meier, L. W. Veldhuizen, and U. Blieske, "Experimental assessment of nanoimprinted textured frontsheets for PV modules," presented at the 8th World Conference on Photovoltaic Energy Conversion, Milan, Sep. 2022. [Online]. Available: https://www.wcpec-8.com/images/2022/-programme/WCPEC-8_Conference_Programme_web-12.pdf

[4] N. Atthi *et al.*, "Fabrication of High Aspect Ratio Micro-Structures with Superhydrophobic and Oleophobic Properties by Using Large-Area Roll-to-Plate Nanoimprint Lithography," *Nanomaterials*, vol. 11, no. 2, Art. no. 2, Feb. 2021, doi: 10.3390/nano11020339.

[5] H. Lan, "Large-Area Nanoimprint Lithography and Applications," in *Micro/Nanolithography - A Heuristic Aspect on the Enduring Technology*, London: IntechOpen, 2018, pp. 43–68. [Online]. Available: https://doi.org/10.5772/intechopen.72860

[6] J. Snieder, M. Dielen, and R. A. van Ostayen, "Elastohydrodynamic lubrication of soft-layered rollers and tensioned webs in roll-to-plate nanoimprinting," *Proceedings of the Institution of Mechanical Engineers, Part J: Journal of Engineering Tribology*, vol. 237, no. 10, pp. 1871–1884, Oct. 2023, doi: 10.1177/13506501231183860.

[7] ASTM C1048-04, "Standard Specification for Heat-Treated Flat Glass - Kind HS, Kind FT Coated and Uncoated Glass."

[8] "COMSOL Multiphysics® v. 6.0. COMSOL AB, Stockholm, Sweden." Accessed: Dec. 15, 2021. [Online]. Available: www.comsol.com/release/6.0

[9] W. Habchi, *Finite element modeling of elastohydrodynamic lubrication problems*. Hoboken, NJ: John Wiley & Sons, 2018.

[10] W. Habchi, D. Eyheramendy, P. Vergne, and G. Morales-Espejel, "Stabilized fully-coupled finite elements for elastohydrodynamic lubrication problems," *Advances in Engineering Software*, vol. 46, no. 1, pp. 4–18, Apr. 2012, doi: 10.1016/j.advengsoft.2010.09.010.

[11] B. J. Hamrock, S. R. Schmid, and B. O. Jacobson, *Fundamentals of fluid film lubrication*, 2nd ed. in Mechanical engineering, no. 169. New York: Marcel Dekker, 2004.

[12] T. V. Kármán, *Festigkeitsprobleme im Maschinenbau*. in Encyklopädie der mathematischen wissenschaften. Teubner, 1910.

[13] A. Fischer, "A special newton-type optimization method," *Optimization*, vol. 24, no. 3–4, pp. 269–284, Jan. 1992, doi: 10.1080/02331939208843795.

[14] C. Liu, "Implementing the Weak Form in COMSOL Multiphysics," COMSOL. Accessed: Oct. 16, 2023. [Online]. Available: https://www.comsol.com/blogs/implementing-the-weak-form-in-comsol-multiphysics/

Acknowledgements

The assistance of Morphotonics is greatly acknowledged. This research was funded by the Topsector Energy Subsidy of the Dutch Ministry of Economic Affairs (TEHE119003).